Magnetic and Mössbauer Investigation of the Photomagnetic Prussian Blue Analogue $Na_{0.32}Co[Fe(CN)_6]_{0.74}\cdot 3.4H_2O$: Cooperative Relaxation of the Thermally Quenched State

S. Gawali-Salunke,[†,‡] F. Varret,[†] I. Maurin,[*,†] C. Enachescu,[§] M. Malarova,[†,||] K. Boukheddaden,[†] E. Codjovi,[†] H. Tokoro,[+] S. Ohkoshi,[+] and K. Hashimoto[+]

Laboratoire de Magnétisme et d'Optique, CNRS-Université de Versailles Saint Quentin, 45, Avenue des Etats-Unis, 78035 Versailles Cedex, France, Department of Chemistry, University of Pune, Pune 411 007, India, Alexandru Ioan Cuza University, Faculty of Physics, Iasi 6600, Romania, Institute of Chemistry, University P. J. Šafárik, Moyzesova 11, 041 54 Košice, Slovakia, and Department of Applied Chemistry, University of Tokyo, 7-3-1 Hongo, Bunkyo, Tokyo 113, Japan

Received: November 18, 2004; In Final Form: February 3, 2005

Thanks to thermal quenching we investigated the relaxation of the metastable state of $Na_{0.32}Co[Fe(CN)_6]_{0.74}\cdot 3.4H_2O$ at low temperature. A self-accelerated process has been observed in agreement with the cooperative character of the system, responsible for the large thermal hysteresis of the charge-transfer-induced spin transition. The mean-field analysis of the relaxation is discussed with respect to the equilibrium properties. A sizable deviation from mean-field behavior is observed at the beginning of the relaxation process, which might be attributed to a preliminary structural relaxation of the quenched state.

1. Introduction

Photocontrol of magnetic properties is an emerging field that would open the way to novel materials functionalities with potential applications in optoelectronics (optical memories, optical isolators, etc.).[1−3] For a more fundamental point of view, it offers the possibility to control magnetic dilution, e.g., by combination of photoexcitation and thermal relaxation.[4] The light-induced magnetic structures have also revealed peculiar features related to the building up of the magnetic correlations without thermal fluctuations, leading to a magnetic metastability of the raw photoexcited state.[5]

In the field of molecular magnets, Prussian blue analogues have provided a wealth of attractive results: high-T_C magnet,[6] photoinduced ferrimagnetism,[1] photocontrolled pole inversion,[2] photo- and thermochromism,[7] second-harmonic generation, etc.[8] $C_xCo[Fe(CN)_6]_y\cdot zH_2O$ analogues, here denoted C−PBAs, where C = Na, K, Rb, and Cs, have been thoroughly studied by various experimental methods: X-ray diffraction,[9] EXAFS,[10] XMCD,[11] magnetic measurements,[12] IR, UV−vis optical absorption,[13] etc. Their (photo)-magnetic properties depend on several factors linked to the chemical environment, namely, the presence of Co^{III}(LS)−Fe^{II}(LS) diamagnetic pairs, leading to Co^{II}(HS)−Fe^{III}-(LS) magnetic pairs by optical electron transfer (LS = low spin, HS = high spin),[14] the presence of $[Fe(CN)_6]$ vacancies in sufficient amount,[15] and the nature of the counterion C;[16] the first two factors are related to the Co/Fe ratio which has to be in the range 1.2−1.4 for efficient photoeffect.[3] A key factor in the photoprocess is the spin transition associated with the nonadiabatic decay of the Co^{II}(LS) excited state, which is responsible for the energy barrier that gives the metastable state a convenient lifetime.

Some of these photomagnetic C−PBAs have shown, in the temperature range 200−300 K, a spontaneous charge-transfer-induced spin transition (CTIST) with thermodynamic features reminiscent of the spin-crossover phenomenon. Thus, Na−PBAs exhibit a first-order transition associated with a rather broad hysteresis loop,[17] indicative of cooperative interactions in the system, while Cs−PBAs show a gradual conversion from the diamagnetic to the magnetic state.[7] For K− and Rb−PBAs a discontinuous CTIST has also been identified but in a limited composition range and with relatively narrow hysteresis.[18] Therefore, a self-accelerated relaxation of the photoexcited state, which is a typical feature of cooperative spin transitions,[19] was expected for cooperative C−PBAs. A first indication of a sigmoidal-type relaxation was reported for $Rb_{0.52}Co[Fe(CN)_6]_{0.84}\cdot 2.3H_2O$, whereas no thermal CTIST was observed up to room temperature.[7,20] In Cs−PBAs the relaxation was not self-accelerated, as expected from the noncooperative character of the CTIST process.[21] No example has been given so far for cobalt hexacyanoferrates which exhibit both the self-accelerated relaxation and an abrupt CTIST.

In the present work we report on relaxation measurements carried out on a thermally quenched $Na_{0.32}Co[Fe(CN)_6]_{0.74}\cdot 3.4H_2O$ sample. The composition has been chosen so as to minimize the temperature interval between the thermal decay of the metastable state and the cooling branch of the thermal hysteresis loop. This situation makes possible a quasi-complete trapping of the high-temperature phase by rapid cooling, as reported in ref 22. An X-ray investigation of the thermally quenched phase of a similar system was recently published[9b] and reports on a crystal structure similar to that of the light-induced phase however with sizable differences in the mean lattice parameter and coherence length values. It is worth noting that crucial events for the quenched system may be spinodal decomposition or (inhomogeneous) nucleation and growth of the relaxed phase. For instance, the rather short diffraction coherence length reported in ref 9b for the quenched phase could be assigned to some relaxation of the sample (∼40%) during

* To whom correspondence should be addressed. Fax: 33-1-39254652. E-mail: imaurin@physique.uvsq.fr.
[†] Laboratoire de Magnétisme et d'Optique.
[‡] University of Pune.
[§] Alexandru Ioan Cuza University.
[||] University P. J. Šafárik.
[+] University of Tokyo.

10.1021/jp044739x CCC: $30.25
Published on Web 04/02/2005

TABLE 1: Selected Mössbauer Data[a]

		Fe^{III} LS (1)			Fe^{II} LS (2)			%
	T	δ(1), mm/s	Γ(1)	ΔE_Q(1), mm/s	δ(2), mm/s	Γ(2)	ΔE_Q(2), mm/s	*A*(1): *A*(2)
1	RT	−0.160(1)	0.460(2)	0.561(3)	*−0.07*	*0.35*	*0.23*	97:03
1	280 K cooling	−0.149(3)	0.570(8)	0.671(9)	*−0.07*	*0.35*	*0.23*	92:08
1	240 K cooling	−0.133(5)	0.50(2)	0.70(1)	*−0.06*	*0.35*	*0.23*	90:10
1	200 K cooling	*−0.11(*)*	*0.52*	0.90(3)	−0.053(2)	*0.35*	0.219(5)	15:85
1	240 K heating	−0.133(9)	*0.52*	*0.7*	−0.068(4)	*0.35*	0.24(1)	48:52
1	280 K heating	−0.147(2)	0.532(8)	0.630(8)	*−0.07*	*0.35*	*0.23*	96:04
1	78 K quenched	−0.081(2)	0.468(8)	0.878(5)	*−0.02*	*0.35*	*0.23*	96:04
2	RT	−0.156(1)	0.390(2)	0.504(2)	*−0.07*	*0.35*	*0.23*	88:12
2	78 K cooling	*−0.073*	0.47(2)	1.02(2)	−0.010(1)	0.322(3)	0.214(1)	11:89

[a] The first column indicates the sample batch. Isomer shift values, δ are quoted relative to α-Fe at room temperature. Γ is the full Lorentzian width at half-maximum, and *A* is the relative area. Italic values were fixed during the fit, and values marked with an asterisk (*) correspond to linearly extrapolated values. Γ(2) was fixed to an averaged value obtained from high statistics Mössbauer experiments under dynamic vacuum, which show large residual Fe^{II}(LS) contributions upon cooling, possibly due to partial/increasing dehydration.

cooling or else during the diffraction measurements. As a consequence, a Mössbauer investigation was first undertaken in order to control the efficiency of our quenching procedure for the compound under study.

2. Experimental Section

The $Na_{0.32}Co[Fe(CN)_6]_{0.74}\cdot 3.4H_2O$ powder sample was prepared from a solution reaction of $CoCl_2$ and $Na_3Fe(CN)_6$ by controlling the NaCl concentration and the temperature. First, $Na_3Fe(CN)_6$ was synthesized by oxidation of $Na_4Fe(CN)_6$ aqueous solution with Cl_2 gas and purified by recrystallization. A mixed aqueous solution of $CoCl_2$ (2×10^{-3} mol·dm^{-3}) and NaCl (1 mol·dm^{-3}) was then slowly added to an aqueous solution of $Na_3Fe(CN)_6$ (2×10^{-3} mol·dm^{-3}) and NaCl (1 mol·dm^{-3}) at 22 °C, which produced a cobalt iron polycyanide precipitate. This precipitate was filtered and dried, yielding a purple microcrystalline powder.

The as-described synthesis procedure was performed twice, and its reproducibility was checked by magnetic measurements. The mass magnetization of the two samples superimposed fairly well, particularly in terms of CTIST temperatures. Chemical characterizations were subsequently carried out on batch 2, whereas all magnetic and Mössbauer measurements presented in the following section refer to batch 1. Elemental analyses, performed by inductively coupled plasma mass spectrometry, yield the nominal formula $Na_{0.32}Co[Fe(CN)_6]_{0.74}\cdot 3.4H_2O$. Infrared spectroscopy measurements, recorded at room temperature using a Shimazu FT-IR 8200PC spectrometer, show two CN stretching bands corresponding to a small amount of Fe^{II} in a $Co^{II}-Fe^{III}$ matrix. The X-ray diffraction pattern, measured with a Rigaku RINT2100 instrument (Cu Kα), evidences a single-phase material within experimental accuracy, with a fcc crystal structure. Calorimetry measurements were performed under N_2, 5 K·min^{-1} scan rate, using a Perkin-Elmer DSC-4 apparatus.

The magnetization curves were recorded using a commercial SQUID magnetometer (Quantum Design MPMS-5). The Mössbauer experiments were performed on a constant-acceleration spectrometer with a 50-mCi source of ^{57}Co in rhodium matrix. Variable-temperature spectra, in the 300−78 K range, were obtained using a standard bath cryostat. Measurements were carried out in the presence of exchange gas (helium) so as to prevent dehydration of the sample. The polycrystalline absorber contained ca. 15 mg of material per square centimeter. The typical experimental line width, in the considered velocity range, was $\Gamma_{exp} = 0.215$ mm·s^{-1}. The spectra, once folded, were fitted without correction for the thickness effect, and least-squares-fitted parameters are given with their standard deviation of statistical origin. The isomer shift of Fe^{II} at room temperature

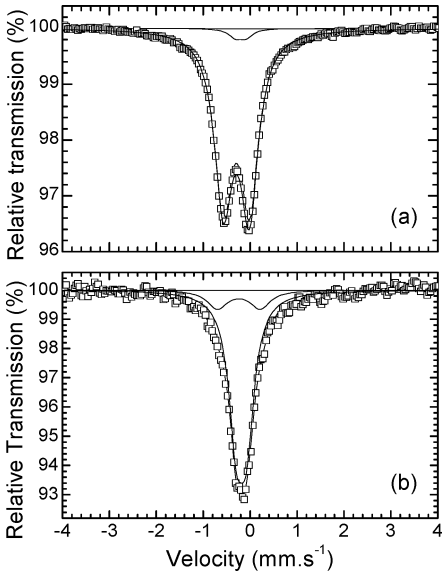

Figure 1. Mössbauer spectra at room temperature (a) and at 200 K after slow cooling under exchange gas (b).

was fixed to a value which corresponds to a compilation of literature data (refs 13 and 16 and references therein). Following the work of Sato et al.,[13] the quadrupole splitting of this species was refined yielding a nonzero value. Attempts to model this contribution using a singlet did not lead to satisfactory fits. Such a nonzero value might reflect some symmetry lowering of the Fe^{II} coordination sphere due to lattice distortions and/or to the random distribution of alkali-metal ions and water molecules in the vicinity of the Fe sites. The Mössbauer parameters obtained for sample batch 2 at selected temperatures are given in Table 1 for comparison.

3. Results and Discussion

Equilibrium Properties. We first describe the equilibrium properties of the system. Mössbauer spectra of the as-received sample at standard temperatures are shown in Figure 1. Hereafter, the $Co^{II}-Fe^{III}$ fraction is assimilated to the relative absorption of the Fe^{III} ion, thus neglecting corrections by the Lamb−Mössbauer factor. The room-temperature (RT) spectrum mainly consists of a doublet, slightly asymmetrical, attributed to the electronic Fe^{III}(LS) state with a small admixture (∼3%) of the Fe^{II}(LS) state. The 200 K spectrum obtained after slow cooling (to avoid frozen-in effects) evidences a clear superimposition of two absorption doublets associated with the coexistence of Fe^{II}(LS) (∼85%) and Fe^{III}(LS) (∼15%) species. The fitted parameters collected for various recording conditions are

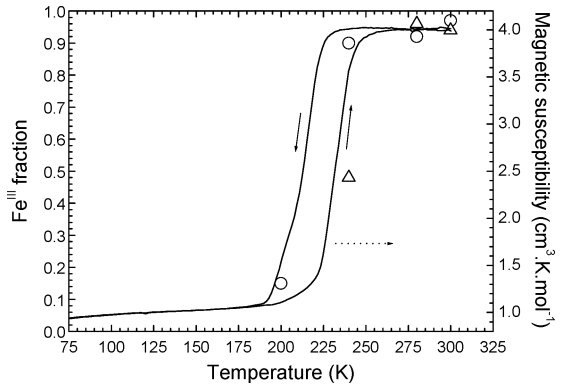

Figure 2. Charge-transfer-induced spin transition from magnetic susceptibility measurements (—), sweep rates ± 0.5 K·min^{-1}, $H = 1000$ G. As-derived transition temperatures are $T_{1/2}^{\uparrow} \approx 232$ K, $T_{1/2}^{\downarrow} \approx 213$ K at one-half population of the switcheable fraction. Open symbols correspond to the Fe^{III} fraction estimated from Mössbauer data in the cooling (○) and subsequent warming (△) modes.

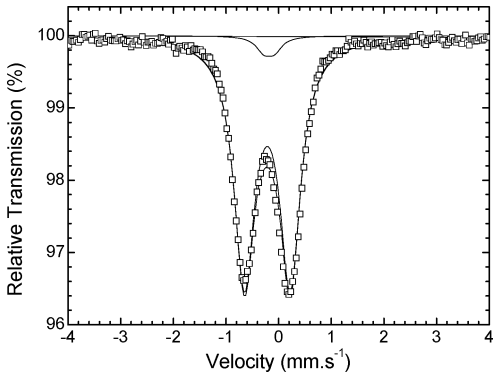

Figure 3. Mössbauer spectrum measured at 78 K after quenching.

listed in Table 1. The as-obtained values are consistent with previous literature data on cobalt hexacyanoferrates[7,13,16,23] and confirm the mechanism of the transition, based on the electron transfer

$$Fe^{III}(LS) + Co^{II}(HS) \rightarrow Fe^{II}(LS) + Co^{III}(LS)$$

$$\text{high-temperature phase: } S(Fe^{III}) = 1/2,\ S(Co^{II}) = 3/2$$

$$\text{low-temperature phase: } S(Fe^{II}) = 0,\ S(Co^{III}) = 0$$

It follows that the system is basically nonmagnetic at low temperature, with parasitic paramagnetism due to residual Co^{II} (HS), and paramagnetic at high temperature. In between a discontinuous CTIST process occurs that involves most of the Co−Fe pairs. Its temperature dependence was more accurately observed by magnetic susceptibility measurements, as reported in Figure 2.

Quenched Metastable State. The successful trapping of the high-temperature state by rapid cooling is illustrated by the Mössbauer spectrum shown in Figure 3 and by the magnetic measurements in Figure 4. Analysis of the Mössbauer data, obtained at 78 K after immersion of the sample in a liquid nitrogen Dewar flask and then transfer into the cryostat, shows no significant Fe^{II} contribution (see Table 1). The large value of the molar susceptibility also confirms that a majority of high-temperature paramagnetic $Co^{II}(HS)-Fe^{III}(LS)$ pairs remain trapped after quenching.

At 0.9 K·min^{-1} sweeping rate the irreversible thermal decay of the quenched state is observed at 160 K, a value similar to that of the photoexcited state.[17] Once trapped at low temperature,

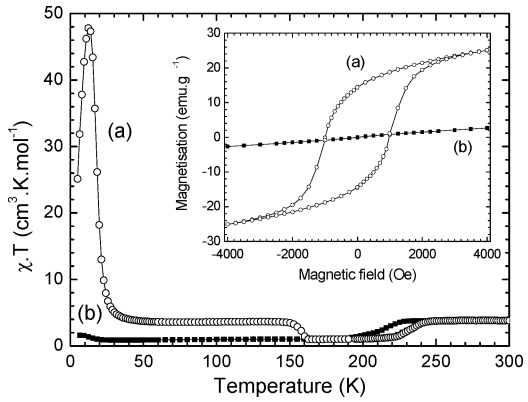

Figure 4. Thermal decay of the quenched state (a) measured in the warming mode at 0.9 K·min^{-1}, $H = 1000$ G. Comparison is made with the slowly cooled state (b). (Inset) *B-H* loops at 5 K.

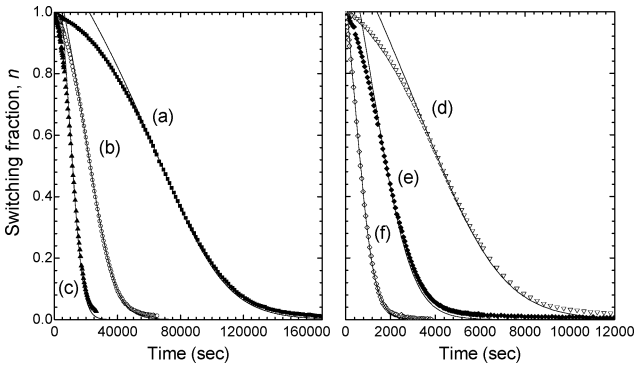

Figure 5. Relaxation of the thermally quenched state measured at several temperatures: (a) 130, (b) 135, (c) 140, (d) 145, (e) 150, and (f) 155 K. Lines correspond to fits to the self-accelerated behavior in the range $0.1 < n < 0.6$.

the high-temperature phase is expected to be ferrimagnetic.[1,11] The susceptibility data χT reported in Figure 4 in addition to the magnetization loop (in inset) are consistent with an onset of magnetic order below 20 K associated with antiferromagnetic couplings.

Relaxation of the Quenched Metastable State. The large hysteresis width reported for the thermal spin transition in Na−PBAs[17] suggests the presence of strongly cooperative interactions between the switcheable units, herein the Co−Fe pairs. Such interactions of steric origin should primarily result from the large bond lengthening (∼0.18 Å[10]) which accompanies the $Co^{III}(LS) \rightarrow Co^{II}(HS)$ electron transfer. As a consequence, relaxation of the $Na_{0.32}Co[Fe(CN)_6]_{0.74}\cdot 3.4H_2O$ quenched phase is expected to exhibit a sigmoidal shape, as extensively documented in the case of spin-crossover solids.[24,25]

Relaxation at various temperatures followed by magnetization measurements is shown in Figure 5. A linear relationship between the product χT and the number of $Co^{II}-Fe^{III}$ pairs, n, was assumed. n was normalized to 1 in the initial state, and $n = 0$ corresponds to the magnetization value measured for the slowly cooled phase at the temperature of the relaxation measurements. In other words, we only follow the switchable fraction of the system, i.e., most of the Co−Fe pairs according to the Mössbauer data. Note that a direct determination of the $Co^{II}-Fe^{III}$ fraction from χT is not straightforward owing the fact that both Co^{II}- and Fe^{III}(LS)-based complexes have a sizable orbital contribution to the magnetic moment; μ spans from 4.5 to 5.2 μ_B for the former,[26] and a standard value for $K_3[Fe(CN)_6]$ is 2.40 μ_B, in clear contrast with the 1.73 μ_B value expected for a spin-only moment.[27] A small relaxation at temperatures slightly lower than that of the measurements cannot be ruled

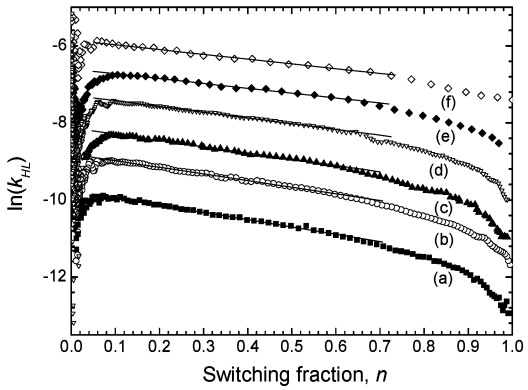

Figure 6. Relaxation rates plotted in logarithmic scale with a linear regression to eq 2.

TABLE 2: Relaxation Parameters of the Quenched Metastable State Derived from the Linear Regression to Eq 2 in the Interval 0.1 < *n* < 0.6

T (K)	130	135	140	145	150	155
$k(T,0)$ (10^5s^{-1})	5.81(2)	14.94(5)	29.4(1)	69.2(3)	136.5(5)	288(3)
$\alpha(T).T$ (K)	246(1)	233(1)	228(2)	216(2)	190(4)	192(4)

out. Such a relaxation should not be larger than that recorded in dynamic mode as shown in Figure 4, so that this effect should be negligible up to 150 K.

Following the simple macroscopic approach developed by Hauser et al. for spin-crossover systems,[24,25] the relaxation rate is related to an energy barrier $E_a(n)$ which is a linear function of the population n of the metastable state; for example, in the thermal activation regime, the relaxation rate follows:

$$k_{HL}(T,n) = k_\infty \exp\left(-\frac{E_a(0) + an}{k_B T}\right) = k_\infty \exp\left(-\frac{E_a(0)}{k_B T}\right) \exp(-\alpha(T)n)$$

with $a = \alpha(T)k_B T$. The self-acceleration parameter, α accounts for an "internal pressure effect" associated with the lattice contraction that accompanies the relaxation process. A convenient analysis of the relaxation curves may be done by deriving the relaxation rate:

$$k_{HL}(T,n) = -\frac{dn(t)}{dt} \quad (1)$$

and plotting the logarithm of k_{HL} as a function of n, which can be written:

$$\ln k_{HL}(T,n) = \ln k(T,0) - \alpha(T)n \quad (2)$$

The experimental data are shown in Figure 6. It must be noted that the relaxation data follow the as-expected linear plot mainly during the second stage of the process, typically $n < 0.6$. Linear regression according to eq 2 was subsequently performed in the range $0.1 < n < 0.6$, and the corresponding data are reported in Table 2. As-derived relaxation curves, obtained by solving eq 1, are displayed as full lines in Figure 5. The remarkable agreement with the mean-field model down to $n \approx 0.1$ indicates the prominent long-range character of the steric interactions in this system. The situation is similar to that of $[Fe(ptz)_6](BF_4)_2$, extensively investigated by Hauser et al.,[24,25] or that of some mixed crystals.[28]

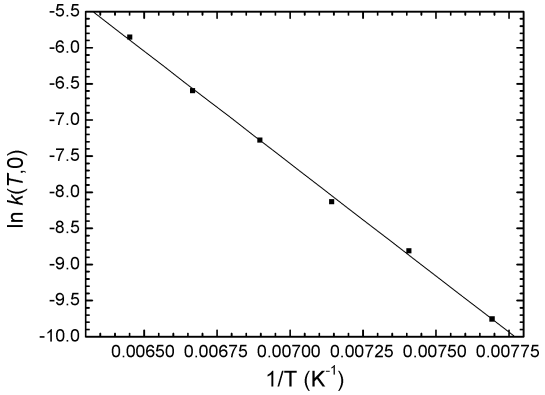

Figure 7. Arrhenius plot of the relaxation rate $k_{HL}(T,0)$ and linear regression yielding the apparent activation energy value $E_a(0) \approx$ 3110(60) K and frequency factor, $k_\infty \approx 1.5(2) \times 10^6$ s^{-1}.

The departures from the linear variation are discussed as follows:

(i) at long times, the slowing down of the relaxation should not be attributed to the onset of correlations created by short-range interactions. In general, this "relaxation tail effect"[29,30] appears more gradually, on a wider n range. Hence, it might instead account for a distribution of barrier energy, E_a, and of self-accelerated coefficient, α, as reported in ref 31 for the case study of compositional inhomogeneities.

(ii) The relatively slower character of the relaxation at short times has not been mentioned so far to our best knowledge. The departure which is usually observed is that of a faster initial relaxation (i.e., the relaxation curve starts as a stretched exponential), interpreted in terms of a distribution of relaxation times, for instance, due to some structural disorder[25] or to the combination of self-accelerated relaxation and inhomogeneous photoexcitation.[32,33] The absence of such an effect in the present curves demonstrates the homogeneity of the initial state, i.e., the complete character of the thermal trapping process. These two aspects will be discussed more quantitatively below.

The mean-field data derived from the relaxation curves in the range $0.1 < n < 0.6$ are consistent with a thermally activated regime (Table 2): $\alpha(T)T$ is roughly constant, and $k_{HL}(T)$ accurately follows a linear Arrhenius plot at constant n value, see Figure 7. The barrier energy and frequency factor were subsequently derived: $E_a(0) \approx 3110(60)$ K, $k_\infty \approx 1.5(2) \times 10^6$ s^{-1}. The barrier energy was also expressed at $n = 1/2$, $E_a(1/2) \approx 3220(80)$ K, to refer to the properties of noninteracting Co−Fe switchable units. Due to the narrow temperature range studied, the above values should be considered as "apparent values", possibly lowered by the proximity of the tunneling regime.[25] For instance, the frequency factor k_∞ value is rather small with respect to the expected time scale, i.e., that of optical vibration frequencies.

To check the relevance of the latter description, we tried to correlate the parameters extracted from the relaxation studies to those related to the CTIST thermal hysteresis analyzed in a mean-field approach using a two-level (Ising-like) model.[34,35] This model previously developed for spin-crossover solids is well known to be formally equivalent[36] to the so-called thermodynamic model[37] based on regular solution theory in the Bragg−Williams approach. Molecules (herein the Co−Fe pairs) are distributed between two states separated by an energy gap, Δ; each state has a degeneracy g_H (g_L) for the high (low) energy state, respectively. Cooperativity is then expressed as an interaction parameter, J, of steric origin. Recent experiments[28] and several models[25,35,38] for spin-crossover systems yield $a =$

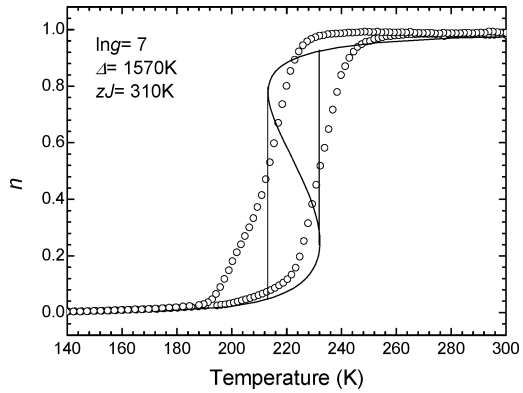

Figure 8. Spontaneous thermal hysteresis loop: experimental data (○) and Ising-like model (—).

$\alpha(T)k_BT = 2zJ$, thus coupling the mechanistic description for relaxation and spontaneous conversion.

Essential features of this widely used model (see ref 39, for instance) are briefly recalled: the equilibrium temperature (approximately the middle of the thermal hysteresis interval) is analytically related to Δ and g

$$T_{1/2} = \Delta/(k_B \ln g) \tag{3}$$

where the parameter $g = g_H/g_L$ can be deduced from calorimetric measurements of the transition enthalpy, ΔH according to $\Delta H = T_{1/2}\Delta S$ and $\Delta S = R \ln g$.[36,40] We measured $\Delta S = 60(10)$ $J\cdot K^{-1}\cdot mol^{-1}$, leading to $\ln g = 7(1)$. The relatively large error bar on ΔH, and hence ΔS, is due to the rather small amount of sample on which the measurements were performed. From the experimental values $T_{1/2} = 222.5$ K and $\Delta T = 19$ K (hysteresis width), we computed the CTIST curve, representative of the fraction of switcheable pairs in the high-energy state, and hence derived the electronic gap and interaction parameter values $\Delta = 1600(300)$ K, $zJ \approx 310(10)$ K (with z being the number of interacting neighbors). As-simulated and experimental curves are shown in Figure 8. Even if considering the error bar for zJ, which mainly originates from the large uncertainty on $\ln g$, the ratio $\alpha(T)T/zJ \approx 220/310 < 1$ drastically departs from the expectation value of 2.

Such a discrepancy demonstrates the inadequacy of the homogeneous mean-field two-level approach in the present case. We turned to an *inhomogeneous* treatment, thus accounting for distributions of the parameters Δ, E_a, and zJ. Indeed, ligand-field distributions associated with the various possible $CoN_{6-x}O_x$ environments were recently invoked to explain the gradual increase in the switcheable fraction upon application of hydrostatic pressure in K− and Cs−PBAs.[41] The presence not only of $Fe(CN)_6$ vacancies but also of alkali-metal ions could participate in the building up of such distributions, as suggested by recent EXAFS studies.[42] Indeed, experiments performed at the alkali-metal edge for a particular Cs−PBA sample have evidenced a displacement of the cesium ions within the tetrahedral sites of the fcc structure while the spin conversion proceeds. As the alkali-ion content was in exact correspondence with the number of Co−Fe switching pairs in this sample, it was claimed that this displacement was the driving force for the transition, in analogy with displacive-type transitions.

Due to the long-range character of the interactions, which has been inferred from the relaxation rate plots of Figure 6, the J-parameter values have to be averaged over large volumes. Consequently, relatively narrow J-parameter distributions are expected. In a first approach we thus merely took into account a distribution of activation energy with the self-acceleration

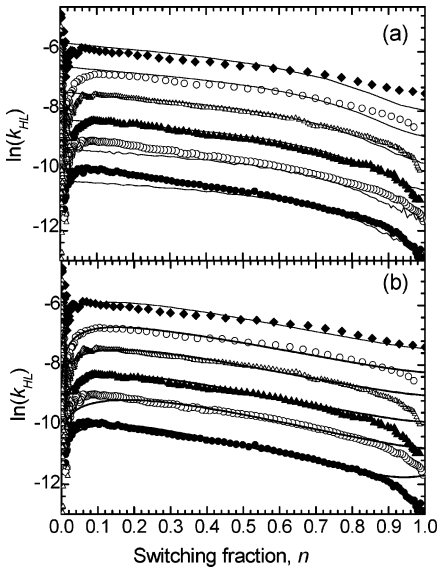

Figure 9. Relaxation rates plotted as in Figure 6 with model curves obeying the constraint $\alpha(T)T = 2zJ = 620$ K and accounting for a barrier energy distribution over independent domains (a) or within a single domain (b).

parameter value fixed to the experimental constraint: $\alpha(T)T = 2zJ = 620$ K.

We first considered inhomogeneities at the long-range scale similar to ref 31, for instance, grains of slightly different chemical composition, that we modeled as independent domains, i presenting a given E_a^i value. Equation 1 is then solved for each domain, and summation is made over all domains. The relaxation slowing down at short times can be fairly well reproduced using a frequency factor, $k_\infty \approx 8 \times 10^6$ s^{-1} and a Gaussian distribution of E_a^i centered on $\langle E_a(1/2)\rangle = 3420$ K with a standard deviation, $\sigma_{Ea} = 50$ K (see Figure 9a). However, the amplitude of this deviation does not decrease on increasing temperature as observed experimentally.

We then used a single-domain model with distributed switching sites. Such a description would better account for a random distribution of point defects ($Fe(CN)_6$ vacancies and/or alkali-metal ions) which locally affect the ligand-field strength and hence the Δ and E_a energy values. A much better agreement with all experimental curves was obtained, see Figure 9b, with the following values: average activation energy, $\langle E_a(1/2)\rangle = 3420$ K, standard deviation, $\sigma_{Ea} = 185$ K, and high-temperature frequency factor, $k_\infty \approx 8 \times 10^6$ s^{-1}. A remarkable result is that the relaxation tails at long times are fairly well reproduced. At short times discrepancies remain but on a narrower n range. We thus suggest the existence of a thermally activated structural evolution prior to (or at the beginning of) the phonon-assisted electronic relaxation, following the recent observation by Hanawa et al.[9b] that sizable structural differences exist between the quenched state and the photoexcited state. The question of the relative stability of these two states is open.

Actually, a complete analysis of the J-parameter distribution should aim to reproduce the true shape of the thermal loop and result in a coherent modeling of both relaxation and spontaneous conversion. It should involve multidimensional parameter distributions, the existence of which was recently shown for spin-transition systems through analysis of the properties of the major and minor hysteresis loops (following Preisach[43] and FORC[44] approaches). The suited investigation is planned. From a general viewpoint it is worth mentioning that the introduction of activation energy distribution induces large changes in the fitted values of the self-accelerated coefficient, α. Presumably,

previous analyses involving similar slowing down in the final stage of the relaxation should be re-analyzed accordingly.

4. Conclusions

As expected, the cooperative nature of the charge-transfer-induced transition for Na-based cobalt hexacyanoferrates has been illustrated by the self-accelerated character of the relaxation of the metastable state obtained by thermal quenching. A qualitative description has been obtained in the frame of the mean-field approximation, leading to the conclusion that the steric interactions essentially have long-range character. However, quantitative agreement with the static regime was not easily obtained and, for instance, required taking into account a distribution of barrier energies. A novel feature, the relatively slower character in the early stage of the relaxation process, has been tentatively ascribed to a preliminary structural evolution. The complex character of the relaxation process is thus strongly supported. Further work would require a detailed comparison with the photoexcited state.

Acknowledgment. We are indebted to the French Ministery of research for supplying a postdoctoral grant (S.G.-S.) and to CNRS (Centre National de la Recherche Scientifique) for financial support. We acknowledge the Laboratoire de Physique de la Matière Condensée, Ecole Polytechnique, for access to the calorimetry measurements.

References and Notes

(1) Sato, O.; Iyoda, T.; Fujishima, A.; Hashimoto, K. *Science* **1996**, *272*, 704.

(2) Ohkoshi, S.; Yorozu, S.; Sato, O.; Iyoda, T.; Fujishima, A.; Hashimoto, K. *Appl. Phys. Lett.* **1997**, *70*, 1040.

(3) Ohkoshi, S.; Hashimoto, K. J. *Photochem. Photobiol., C: Photochem. Rev.* **2001**, *2*, 71.

(4) Goujon, A.; Varret, F.; Escax, V.; Bleuzen, A.; Verdaguer, M. *Polyhedron* **2001**, *20*, 1347.

(5) Varret, F.; Constant-Machado, H.; Dormann, J. L.; Goujon, A.; Jeftic, J.; Dolbecq, A.; Verdaguer, M. *Hyperfine Interact.* **1998**, *113*, 37. Varret, F.; Goujon, A.; Bleuzen, A. *Hyperfine Interact.* **2001**, *134*, 69.

(6) Ferlay, S.; Mallah, T.; Ouahes, R.; Veillet, P.; Verdaguer, M. *Nature* **1995**, *378*, 701.

(7) Goujon, A.; Varret, F.; Escax, V.; Bleuzen, A.; Verdaguer, M. *Polyhedron* **2001**, *20*, 1339.

(8) Ikeda, K.; Ohkoshi, S.; Hashimoto, K. *J. Electrochem. Soc.* **2002**, *149*, E445.

(9) (a) Escax, V.; Bleuzen, A.; Itié, J. P.; Munsch, P.; Varret, F.; Verdaguer, M. *J. Phys. Chem B* **2003**, *107*, 4763. (b) Hanawa, M.; Moritomo, Y.; Kuriki, A.; Tateishi, J.; Kato, K.; Takata, M.; Sakata, M. *J. Phys. Soc. Jpn.* **2003**, *72*, 987.

(10) (a) Cartier dit Moulin, C.; Villain, F.; Bleuzen, A.; Arrio, M. A.; Sainctavit, P.; Lomenech, C.; Escax, V.; Baudelet, F.; Dartyge, E.; Gallet, J. J.; Verdaguer, M. *J. Am. Chem. Soc.* **2000**, *122*, 6653. (b) Yokohama, T.; Kiguchi, M.; Ohta, T.; Sato, O.; Einaga, Y.; Hashimoto, K. *Phys. Rev. B* **1999**, *60*, 9340.

(11) Champion, G.; Escax, V.; Cartier dit Moulin, C.; Bleuzen, A.; Villain, F.; Baudelet, F.; Dartyge, E.; Verdaguer, M. *J. Am. Chem. Soc.* **2001**, *123*, 12544.

(12) Pejaković, D. A.; Manson, J. L.; Miller, J. S.; Epstein, A. J. *Phys. Rev. Lett.* **2000**, *85*, 1994.

(13) Sato, O.; Einaga, Y.; Fujishima, A.; Hashimoto, K. *Inorg. Chem.* **1999**, *38*, 4405.

(14) Bleuzen, A.; Lomenech, C.; Escax, V.; Villain, F.; Varret, F.; Cartier dit Moulin, C.; Verdaguer, M. *J. Am. Chem. Soc*. **2000**, *122*, 6648.

(15) Escax, V.; Bleuzen, A.; Cartier dit Moulin, C.; Villain, F.; Goujon, A.; Varret, F.; Verdaguer, M. *J. Am. Chem. Soc.* **2001**, *123*, 12536.

(16) Sato, O.; Einaga, Y.; Iyoda, T.; Fujishima, A.; Hashimoto K. *J. Phys. Chem. B* **1997**, *101*, 3903.

(17) Shimamoto, N.; Ohkoshi, S.; Sato, O.; Hashimoto, K. *Inorg. Chem.* **2002**, *41*, 678.

(18) Escax, V. Ph.D. thesis, Université Pierre et Marie Curie, Paris 2002.

(19) Gütlich, P.; Hauser, A.; Spiering, H. *Angew. Chem., Int. Ed. Engl*. **1994**, *33*, 2024.

(20) Goujon, A.; Roubeau, O.; Varret, F.; Dolbecq, A.; Bleuzen, A.; Verdaguer, M. *Eur. Phys. J. B* **2000**, *14*, 115.

(21) Varret, F.; Goujon, A.; Boukheddaden, K.; Nogues, M.; Bleuzen, A.; Verdaguer, M. *Mol. Cryst. Liq. Cryst.* **2002**, *379*, 333.

(22) Shimamoto, N.; Ohkoshi, S.; Sato, O.; Hashimoto, K. *Mol. Cryst. Liq. Cryst*. **2000**, *344*, 95.

(23) (a) Einaga, Y.; Ohkoshi, S.; Sato, O.; Fujishima, A.; Hashimoto, K. *Chem. Lett.* **1998**, 585. (b) Monaghan, C. P.; Fanning, J. C. *J. Phys. Chem*. **1978**, *82*, 1045. (c) Reguera, E.; Bertran, J. F. *Hyperfine Interact*. **1994**, *88*, 49.

(24) Hauser, A.; Gutlich, P.; Spiering, H. *Inorg. Chem.* **1986**, *25*, 4245.

(25) Hauser, A.; Jeftic, J.; Romstedt, H.; Hinek, R.; Spiering, H. *Coord. Chem. Rev.* **1999**, *190*−*192*, 471.

(26) Martin, D. H. In *Magnetism in Solids*; Iliffe: London, 1967; p 205.

(27) Tweedle, M. F.; Wilson, L. J. *J. Am. Chem. Soc.* **1976**, *98*, 4824.

(28) Enachescu, C.; Linares, J.; Varret, F. *J. Phys.: Condens. Matter* **2001**, *13*, 2481.

(29) Romstedt, H.; Hauser, A.; Spiering, H. *J. Phys. Chem. Solids* **1998**, *59*, 265.

(30) Hôo, B.; Boukheddaden, K.; Varret, F. *Eur. Phys. J. B* **2000**, *17*, 449.

(31) Roubeau, O.; Haasnoot, J. G.; Linarès, J.; Varret, F. *J. Mol. Cryst. Liq. Cryst* **1999**, *335*, 1253.

(32) Hauser, A.; Adler, J.; Gütlich, P. *Chem. Phys. Lett*. **1988**, *152*, 468.

(33) Varret, F.; Nogues, M.; Goujon, A. In *Magnetism: Molecules to Materials, Part II*; Miller, J., Drillon, M., Eds.; Wiley WCH: New York, 2001; p 257.

(34) (a) Wanjflasz, J.; Pick, R. *J. Phys. France* **1971**, *32*, C1. (b) Bousseksou, A.; Nasser, J.; Linares, J.; Boukheddaden, K.; Varret, F. *J. Phys. I* **1992**, *2*, 1381.

(35) Boukheddaden, K.; Shteto, I.; Hôo, B.; Varret, F. *Phys. Rev. B* **2000**, *62*, 14796.

(36) Zimmerman, R.; Konig, E. *J. Phys. Chem. Solids* **1977**, *38*, 779.

(37) Slichter C. P.; Drickamer H. G. *J. Chem. Phys.* **1972**, *56*, 2142.

(38) (a) Adler, P.; Hauser, A.; Vef, A.; Spiering, H.; Gütlich, P. *Hyperfine Interact.* **1989**, *47*, 343. (b) Willembacher, N.; Spiering, H. *J. Phys. C* **1988**, *21*, 1423.

(39) Varret, F.; Gawali-Salunke, S.; Boukheddaden, K.; Bousseksou, A.; Codjovi, E.; Enachescu, C.; Linares, J. *C. R. Chim.* **2003**, *6*, 395.

(40) Sorai, M. *Chem. Soc. Jpn.* **2001**, *74*, 2223.

(41) Ksenofontov, V.; Levchenko, G.; Reiman, S.; Gutlich, P.; Bleuzen, A.; Escax, V.; Verdaguer, M. *Phys. Rev. B* **2003**, *68*, 24415.

(42) Bleuzen, A.; Escax, V.; Ferrier, A.; Villain, F.; Verdaguer, M.; Munsch, P.; Itié, J. P. *Angew. Chem., Int. Ed* **2004**, *43*, 3728.

(43) Enachescu, C.; Constant-Machado, H.; Menendez, N.; Codjovi, E.; Linarès, J.; Varret, F.; Stancu, A. *Physica B* **2001**, *306*, 155.

(44) Tanasa, R.; Enachescu, C.; Stancu, A.; Linares, J.; Codjovi, E.; Varret, F. *Phys. Rev. B* **2005**, *71*, 14431.